Controlled release of chlorhexidine from a HEMA-UDMA resin using a magnetic field

Dong Luo[a], Saroash Shahid[b], Samiul Md. Hasan[c], Robert Whiley[c],

Gleb B. Sukhorukov[a], Michael J. Cattell[b*]

[a]School of Engineering and Materials Science, Queen Mary University of London, London, Mile End Road, E1 4NS, UK.

[b] Centre for Oral Bioengineering, Bart's and the London, School of Medicine and Dentistry, Queen Mary University of London, Turner Street, Whitechapel, E1 2AD, UK.

[c]Centre for Oral Immunobiology and Regenerative Medicine, Bart's and the London, School of Medicine and Dentistry, Queen Mary University of London, Blizzard Building, 4 Newark Street, E1 2AT, London, UK

[*]corresponding author; email address: m.cattell@qmul.ac.uk

Abstract

Objectives: To functionalise novel chlorhexidine (CHX) particles with iron oxide (Fe_3O_4) nanoparticles and control their release kinetics in a dental resin using an external magnetic field.

Methods: Fe_3O_4 nanoparticles were synthesized and incorporated into spherical CHX particles and the powder was freeze dried. Resin disc specimens were produced using a UDMA-HEMA resin mixed with freeze dried spherical Fe_3O_4-CHX particles (5 wt. %), which were placed into a Teflon mould (10 mm diameter × 1 mm depth) and covered with a Mylar strip. A MACS magnet was left in contact for 0 mins (Group 1), 5 mins (Group 2) or 10 mins (Group 3) and the resin discs subsequently light cured (Bluedent LED pen, Bulgaria) for 60 s per side. The resin discs were immersed in deionised water at various time points up to 650 h. UV-Vis absorbance was used to determine the CHX content. CHX released for each time point was determined. The functionalized CHX particles and resin discs were characterized using TEM, TGA, EDX and SEM.

Results: Fe_3O_4 nanoparticles (20 nm) incorporated into the spherical CHX particles, led to a mean (SD) particle size reduction from 17.15 (1.99) µm to 10.39 (2.61) µm. The presence of Fe_3O_4 nanoparticles in the spherical CHX particles was confirmed with SEM, EDX, and TGA. SEM of group 1 resin discs (no magnetic exposure) showed functionalized CHX spheres were homogeneously distributed within the resin discs. For resin discs which had magnetic exposure (5 or 10 mins) the particles started to cluster nearer the surface (Group 2: 43.7%, Group 3: 57.3%), to a depth of 94 µm. UV-Vis absorbance revealed Group 1 resin discs had a cumulative CHX release of 4.4% compared to 5.9 % for group 2 and 7.4% for group 3 resin discs, which had magnetic exposure (5, 10 mins).

1. Introduction

Antibacterial agents and their delivery are of great importance in medicine and dentistry, since a wide range of bacterial infections are still the major reasons for recurrent/ persistent infections despite the use of antibiotics [1, 2]. Biomaterial implants used in modern medicine for functional restorations are also susceptible to infections, which can lead to failure [3]. Increased application of implants in dentistry has led to significant numbers of patients developing peri-implantitis (47.1% prevalence with mean functional loading of 10 years) [4]. These painful infections are caused by anaerobic bacteria and lead to bone loss, exposure of titanium implant threads and ultimately implant removal. Painful surgical treatment, smoothing of the implant [5] and cleaning together with antibiotic therapy can be carried out, but many of these treatment strategies have poor outcomes [6]. The site of bacterial infections can also be largely inaccessible to antimicrobial agents used in the oral cavity, especially in periodontal pockets and proximal/marginal areas of composite restorations, which are susceptible to bacterial micro-leakage. This can lead to the establishment of bacterial biofilms causing secondary caries, inflammation and degradation of the polymer composite [7]. Bacteria may become resistant if the antibacterial agents cannot penetrate the biofilm and if sufficient drug is not available at the infection site [8, 9]. Therefore efficient delivery and penetration of the antibacterial agent to the exact site of infection is highly desirable. In some infection, enhanced antimicrobial drug delivery might be achieved by using a non-invasive external magnetic force to improve drug navigation to the infection site. Magnetic field navigated drug delivery is based on the use of magnetic nanoparticles such as magnetite, strontium ferrite, manganese ferrite and others [10] embedded into different nano-/micro- carriers or used directly, and various therapeutic agents have been loaded for magnetic targeted delivery [11-14]. Recent studies have demonstrated that by using a magnetic field superparamagnetic iron oxide nanoparticles are able to target infection sites, inhibit several bacterial functions and penetrate biofilms; thereby overcoming

the therapeutic barrier often encountered when using traditional antibiotics or other antibacterial agents [3, 9]. In dentistry, magnetic nanoparticles have been incorporated into polymeric scaffolds or cement composites to enhance cell adhesion and osteogenic differentiation [15-17] and have been navigated inside dental tubules via an external magnetic field for treating dental hypersensitivity [18]. Magnetic nanoparticles are also combined with other components to enhance their antibacterial performance. Mahmoudi et al., reported core-shell nanoparticles consisting of a superparamagnetic core and silver shell, which showed enhanced antimicrobial activities and excellent penetration of biofilms when an external magnetic field was applied [19].

CHX is a bis-biguanide antiseptic and disinfectant extensively used in medicine and dentistry [20, 21]. The current authors previously developed a novel formulation of CHX with a controllable crystal size [22] and release behavior when incorporated into a dental resin [23]. Functionalisation of the novel CHX particles with gold nano-rods resulted in the ability to produce a near-infrared light (NIR) responsive CHX release [24]. With the ability to move CHX to an infection site using an external magnetic field, the combination of magnetic nanoparticles with CHX crystals could extend the range of antibacterial applications and improve efficacy. Therefore we aim to functionalise the novel CHX particles with iron oxide nanoparticles (Fe_3O_4) and investigate the possibility of moving the resulting CHX composite in a dental resin with an external magnetic field. There are many clinical situations where a targeted drug release would be desirable in restorative dentistry, periodontology and medicine. Magnetic responsive CHX formulations may be particularly useful in developing magnetic targeted antibacterial materials.

2. Materials and Methods

2.1 Magnetic nanoparticles synthesis

Iron oxide nanoparticles (Fe_3O_4) were synthesized according to a well-established Massart's co-precipitation method [25]. Briefly, 2.35g $FeCl_3$ (Fluka, 44944, Lot: 30607125) and 0.86g $FeCl_2$ (Fluka, 44939, Lot: 24606139) were added in 40 ml H_2O in a three-neck flask, and then placed in an oil bath and heated up to 80 ^oC in an argon atmosphere. The mixture was next stirred using a magnetic stirrer (VWR Stirrer, USA), at a rate of 800 rpm, whilst 5 ml NH_4OH (Sigma-Aldrich, UK, lot: 320145) was added slowly with a syringe. Heating was maintained at 80 ^oC for 30 mins and then 2 ml of 0.5g/ml citric acid (Sigma-Aldrich, UK, 27490, Lot: 23405C03) was introduced. The temperature was next raised to 95 ^oC and held for 90 mins. The product was cooled and dialysed against H_2O in a 14 kDa cut-off membrane (Sigma-Aldrich, UK, D9527) for one week. The Fe_3O_4 nanoparticles were then characterized using transmission electron microscopy (TEM) (JEOL-JEM 2010, USA) at acceleration voltage of 200 kV.

2.2 Fe_3O_4-Chlorhexidine sphere synthesis

Spherical CHX particles (SCPs) were functionalized with Fe_3O_4 nanoparticles and prepared by mixing 200 µl of Fe_3O_4 nanoparticle suspension with 1 ml of 0.33M $CaCl_2$ (Sigma-Aldrich, UK, C8106, Lot: SLBF7416V). The mixture was added to 1 ml of 15 mg/ml CHX-diacetate solution (Sigma-Aldrich, UK, C6143, Lot: 19H0417). The mixtures were shaken for 1 min, and then centrifuged at 2000 rpm for 1 min (Eppendorf centrifuge, 5417C, Germany). To reduce the dissolution of the particles, the precipitates were washed three times with 0.33M $CaCl_2$ solution. All the supernatants were collected for UV-Vis absorbance (Wavelength = 254 nm). The functionalized CHX spheres (CHX/Fe_3O_4) were freeze dried (ScanVac Cool Safe Freeze Drying, Denmark) at -107 ^oC, 0.009 mBar for 1 day. The proportion of CHX in the

powders was calculated using both UV-Vis (Lambda 35, Perkin Elmer, USA) and thermo-gravimetric analysis (TGA Q50) as described in our previous work [23]. Control SCPs (without Fe_3O_4 nanoparticles) were synthesized by co-precipitation of $CaCl_2$ and CHX-diacetate, as described in our previous study [26].

2.3 Preparation of functionalized chlorhexidine UDMA- HEMA resin discs

UDMA-HEMA resin was prepared by mixing 64% urethane dimethacrylate (UDMA) (Esschem, UK, Lot: 591-22), 36% hydroxyethyl methacrylate (HEMA) (Aldrich, UK), 0.08% of N, N-dimethyl-P-toluidine (Acros Organics, UK) and 0.05% dimethylamino ethyl methacrylate (Aldrich, UK). The mixture was stirred at 800 rpm for 15 min (VWR Stirrer, USA). Finally, camphorquinone (Sigma-Aldrich, UK) was added at the proportion of 0.1% and the mixture was stirred for another 15 min. The viscous liquid resin was next mixed for 1 min with the freeze dried CHX/Fe_3O_4 spheres (5 wt.% CHX content) using a Rotomix (120V/60Hz, 2850 rotations/min) (ESPE RotoMix, USA).

The resin mixture containing CHX/Fe_3O_4 spheres was placed into a Teflon mould (10 mm in diameter ×1 mm depth), left for 10 mins and then cured through a Mylar film with a curing light (Bluedent LED pen, Bulgaria) (430-490nm, 600 mW/sq.cm) for 60 s on both sides (Group 1). To control the distribution of CHX/Fe_3O_4 particles in the resin mixture, it was again placed into the Teflon mould and covered with a Mylar film. A MACS magnet (1.5 cm diameter, 0.5 cm depth, Miltenyi Biotech, UK) was left in contact for 5 mins (Group 2) or 10 mins (Group 3) and then the resin discs were light cured for 60 s per side. All the discs were next weighed on a microbalance (Salter Ander-180A weighing scale, UK) and the amount of CHX in each disc was calculated.

2.4 UV/VIS Spectroscopy

The release kinetics of CHX from the resin discs was measured using UV-Vis absorption (Lambda 35, Perkin Elmer, USA). All the UDMA-HEMA resin discs containing CHX/Fe_3O_4 spheres were kept in cuvettes containing 2 ml deionized water at room temperature. Specimen Groups 1, 2 and 3 (n=3 per group) were tested at time points of 1h, 3h, 5h, 15h, 25h, 40h, 65h, 95h, 140h, 205h, 275h, 350h, 500h and 650h. Solutions from each time interval were collected for the UV-vis absorbance test and replaced with fresh deionised H_2O. The released CHX for each time point was determined according to an established calibration curve [23]. Residual CHX in all the supernatants was determined by measuring the UV absorption of the supernatants at 254 nm. Cumulative release for each of the groups was plotted and compared.

2.5 Scanning electron microscopy (SEM) characterization

The spherical CHX particles, CHX/Fe_3O_4 spheres and resin discs containing CHX/Fe_3O_4 spheres (Groups 1-3) were characterised using SEM. The resin discs containing CHX/Fe_3O_4 spheres were immersed in liquid nitrogen and fractured to analyse the distribution of spheres. All the samples were gold coated for 45s at 18 mA, 0.04 mBar using a sputter coater (SC7620, Emitech, UK) and viewed using a scanning electron microscope (FEI Inspect-F, USA), in the secondary electron imaging mode, with an accelerating voltage of 10 kv and spot size of 3.5. To identify the presence of Fe in the CHX/Fe_3O_4 spheres, energy dispersive X-ray spectroscopy (EDX), (INCA, Oxford Instruments, High Wycombe, UK) was used with an accelerating voltage of 20 kV, working distance of 10 mm and spot size of 5. Back scattered SEM images were also used to illustrate the distribution of Fe in the CHX/Fe_3O_4 spheres.

To determine the influence of Fe_3O_4 nanoparticles on the size of spherical CHX particles, the Mean (SD) particle diameter of the spherical CHX particles and functionalized CHX particles

(CHX/Fe_3O_4) were measured using quantitative image analysis software (Nano Measurer, version 1.2) of the SEM images.

Resin discs containing CHX/Fe_3O_4 spheres with 0 mins (Group 1), 5 mins (Group 2) or 10 mins (Group 3) magnetic exposure were characterized using SEM using the above protocol. To acquire a panoramic image, cross-sectional SEM images were taken continuously from one side of the resin disc to the other side and then all the individual images were assembled to produce a panoramic image. To analyze the distribution of CHX/Fe_3O_4 spheres in the resin discs as a function of distance to the magnet, the panoramic images for each group (n=3 per group) were divided into 21 frames. Each frame was presented along the x-axis in 47 µm increments. The number of CHX/Fe_3O_4 spheres in each of the frames was counted and summed to get the total number. The CHX/Fe_3O_4 sphere distribution in the resin discs was plotted as a function of frame distance to the magnet side, with each point representing the percentage of CHX particles in each frame accordingly. The border of the frame next to the magnet was set as zero.

In order to assess the influence of magnetism on particle distribution the number of CHX/Fe_3O_4 particles in each frame (n=3 in each of the three test groups) were statistically compared using a one way ANOVA ($p<0.05$, Tukey test, Sigma stat, version 2.03, SPSS Inc.).

2.6 Cytotoxicity Assay

The Cytotoxicity of CHX/Fe_3O_4 spheres were evaluated with a standard MTT (3-[4,5 dimethylthiazol-2-yl]-2, 5 diphenyl tetrazolium bromide) assay using L929 fibroblast cell line (ECACC 85011425, UK). The MTT assay was carried out according to the protocol outlined in ISO 10993-5:2009 (Biological evaluation of medical devices - Part 5: Tests for in vitro cytotoxicity). Cells were cultured in Dulbecco's Modified Eagle's Medium (DMEM; Lonza, UK) supplemented with 10% fetal bovine serum (FBS) with 100 IU/mL penicillin, 100 µg/ml streptomycin, and 2 mmol/L glutamine (all from Invitrogen, UK) in a humidified incubator in 10% CO2 in air at 37°C seeded in flat bottom 96-well microtiter plates (Sarstedt, Germany) at 10^4 cells per well with a final volume of 225µl and incubated for 22 hours. Following incubation, a series of 2 fold dilutions (0.000625 % to 0.08 %) of CHX/Fe_3O_4, commercial chlorhexidine diacetate (CHX) and pure Fe_3O_4 nanoparticles in deionised water were prepared. 25µl of each CHX/Fe_3O_4, CHX and pure Fe_3O_4 nanoparticle concentration was added into respective 96-well flat-bottomed microtiter plates to achieve a final CHX/Fe_3O_4, CHX and pure Fe_3O_4 nanoparticle concentration range of 0.0000625 % to 0.008 %. 25µl of sterile deionized water were added into the control wells (cells only and medium only) and plates were incubated for 24 hours. Culture medium containing the treatments was then removed and 50 µL of 1 mg/mL tetrazolium salt MTT (Sigma-Aldrich, Gillingham, UK) was added to each well and incubated in 37 °C for 2 hours. Formazan crystals generated by mitochondrial enzyme activity were then dissolved by 100 µl of isopropanol and the intensity of the purple coloured reaction product was quantified by measuring the absorbance spectra with a plate reader at 570 nm. The absorbance of untreated cells was considered to be 100%. Relative cell viability was calculated as: (absorbance of treated cells/absorbance of untreated cells) x 100%. Finally, an inverted microscope (Nikon Eclipse TE2000-S, UK) was used to image the morphology of treated and untreated cells.

2.7 Antimicrobial Assay

Oral pathogenic bacterium, *Porphyromonas gingivalis* (strain W50) was used to evaluate the antibacterial activity of CHX/Fe_3O_4. *P. gingivalis* was grown on blood agar (Blood Agar Base No. 2; Oxoid, UK) plates in an anaerobic atmosphere (10% H_2, 10% CO_2, and 80% N_2) at 37°C for 48 hours. The bacterial culture was harvested and suspended in brain heart infusion (BHI) broth (CM1135; Oxoid, UK) supplemented with 5µg/ml haemin and 5µg/ml menadione bisulphite. The bacterial culture was then grown for 24 hours anaerobically after which it was adjusted to an initial optical density (OD) of 0.1 at 600 nm (OD_{600nm}) with BHI broth. A series of 2 fold dilutions (from 0.08 % to 0.000625 %) of CHX/Fe_3O_4 in deionised water were prepared. 225µl of diluted bacteria and 25µl of each CHX/Fe_3O_4 concentration was mixed into 96-well flat-bottomed microtiter plates to achieve a final CHX/Fe_3O_4 concentration range of 0.008 % to 0.0000625 %. For control wells (bacterial suspension only and BHI only), 25µl of sterile deionized water were added. The plates were incubated for 24 hours anaerobically and OD was determined at 595 nm (OD_{595nm}) to quantify bacterial growth. The lowest CHX/Fe_3O_4 concentration with no detectable bacterial growth was recorded as the minimum inhibitory concentration (MIC). Additionally, MTT assay was carried out as described above to determine the viability of treated bacteria. Briefly, bacterial culture medium containing different CHX/Fe_3O_4 concentrations were removed, 50 µL of 1 mg/mL tetrazolium salt MTT (Sigma-Aldrich, Gillingham, UK) was added to each well and incubated anaerobically for 2 hours. Formazan crystals were then dissolved with 100 µl of isopropanol and absorbance was measured at 570 nm. Bacterial viability was calculated as: absorbance of treated bacteria/absorbance of untreated bacteria x 100%.

3. Results

3.1 Results of the TEM study

TEM image of synthesized Fe_3O_4 nanoparticles is showed in Figure 1. It can be seen that the mean diameter (SD) of the nanoparticles is 13.1 (2.4) nm and they appeared in clusters.

3.2 Results of the SEM study

SEM photomicrographs of the SCP and CHX/Fe_3O_4 spheres is shown in Figure 2a, e and 2b, f. Spherical CHX particles were produced by co-precipitation of chlorhexidine diacetate and $CaCl_2$. Both samples showed a porous structure and particles were monodispersed (Figs. 2a-f). The mean (SD) diameter for SCP was 17.15 (1.99) µm, whilst the CHX/Fe_3O_4 spheres had a mean (SD) diameter of 10.39 (2.61) µm. SEM photomicrographs at high magnification (×40,000) indicated a dendritic structure for both particles (Figs. 2c-d), but Fe_3O_4 nanoparticles appeared dispersed within the structure for the functionalized particle (Fig. 2d). SEM images in the back scattered mode illustrated the presence of Fe in the CHX/Fe_3O_4 spheres (Fig. 2f), which was not present in the SCP (Fig. 2e) and peaks for Fe were clearly identified using EDX (Fig. 3).

The cross-sectional SEM images of resin discs (Groups 1-3) assembled to make panoramic images are presented in Figures 5a, b, c. Frames (indicated by white lines, first 3 numbered) are presented in 47 µm increments and the position of the magnet (M) is marked to indicate the magnet side. For the Group 1 resin discs with no magnetic exposure (Fig. 5a), the CHX/Fe_3O_4 spheres were homogeneously distributed throughout the resin discs. The Group 2 and 3 specimens (5 and 10 mins magnetic exposure) resulted in the clustering of many of the CHX/Fe_3O_4 spheres at the magnet end (Figs. 5b, c). According to the numbers of magnetic CHX/Fe_3O_4 spheres counted in each of the frames, their distribution was plotted as a function of distance from the magnet (Figs. 6 a, b, c). To gauge the effects of the magnetic field the

percentage of particles in the first three frames (nearest the magnet) and in the disc with no treatment are listed. Group 1 frames were; 1: 8.4 %, 2: 3.6 % and 3: 7.1 % (Fig 6a). Group 2 (5 min magnetic exposure) frames were; 1: 22.9%, 2: 20.8%, 3: 7.1% and Group 3 (10 min magnetic exposure) were 1: 38%, 2: 19.3% and 3: 5.5% (Figs 6 b, c). The results of the statistical analysis of particles in the SEM frames (1-3) were highly significant ($p<0.01$) and are given in Table 1. The power of the performed test with alpha was 0.050:1.0.

3.3 Results of the Thermo-gravimetric analysis

The results of the TGA analysis are shown in Figure 4. The spherical CHX particles (SCP) had 8.5 wt.% remaining after increasing the temperature to 800 ^{o}C [24], and for the Fe_3O_4 functionalized CHX spheres there was 33 wt.% remaining.

3.4 Release kinetics of CHX from resin

The release of CHX from the HEMA-UDMA resin discs containing functionalized CHX/Fe_3O_4 spheres (Groups 1-3), demonstrated a two stage process (Fig. 7). In the first stage there was a burst release (until 200 h) which was more rapid for Groups 2 and 3 when compared to Group 1. The second stage of the plots demonstrated a sustained release for all groups. Group 1 (no magnetic treatment) resulted in 4.4% CHX released, whilst Group 2 (5 min magnetic treatment) gave 5.9% CHX released and Group 3 (10 min magnetic treatment) resulted in 7.4% CHX released at 650 h.

3.5 Cytotoxicity Assay Results

The results of the cytotoxicity assay are presented in Figure 8a. Treatment with functionalized chlorhexidine spheres (CHX/Fe_3O_4) and commercial chlorhexidine diacetate (CHX) reduced cell viability in a dose-dependent manner *in vitro*. Overall, CHX/Fe_3O_4 spheres demonstrated reduced cytotoxicity in comparison with CHX at the same concentration.

Relative cellular viability was reduced to approximately 50% in 0.0005% CHX treated cultures whilst the viability was above 80% in CHX/Fe_3O_4 sphere treated cells. While viability remained >70% in CHX/Fe_3O_4 sphere treated cells at 0.001% concentration, CHX treated cells demonstrated reduced viability (~30%) (Fig.8a). Accordingly, changes in cellular morphology (rounded, swelled, and loss of attachment to the wells) were also observed in both 0.0005% and 0.001% CHX treated cultures, whilst the normal morphology was maintained in CHX/Fe_3O_4 sphere treated cultures (Fig. 8b-d).

3.6 Antimicrobial Assay Results

Figure 9 shows the antimicrobial activity of CHX/Fe_3O_4 against *P.gingivalis*. The growth of *P. gingivalis* was completely inhibited by 0.0005% wt./vol. CHX/Fe_3O_4 (MIC) (Figure 9a) as measured by culture optical density. The MTT assay also confirmed this MIC value with no viability being detected at 0.0005% wt./vol. CHX/Fe_3O_4 (Figure 9b).

4. Discussion

The antibacterial activities of metal nanoparticles such as gold, silver, copper, zinc and titanium and their applications against bacterial infections are well established [27]. In the current study Fe_3O_4 nanoparticles with an mean (SD) diameter of 13.1 (2.4) nm (Fig. 1) were synthesized using a co-precipitation method to take advantage of their ferrimagnetic properties [28] and allow targeted CHX drug release. Magnetic nanoparticles are extensively used for targeted drug delivery and as diagnostic agents due to their excellent magnetic properties, superior biocompatibility and ease of functionalization [14]. Magnetite (Fe_3O_4) is an inverse spinel structure with various particle morphologies that include spherical, octahedral or cubic structures [29]. The cubic structure is known to grow via a screw dislocation process [30]. In this study TEM of the precipitated Fe_3O_4 nanoparticles appeared to show signs of spherical morphology, although this was indistinct. The shape, size and surface chemical functionalities of iron oxide nanoparticles have a profound effect on their antibacterial activities [3]. When tested, CHX/Fe_3O_4 demonstrated antimicrobial activity against the periodontal pathogen *P. gingivalis* (Fig. 9). Importantly the cytotoxicity assay results showed that the CHX/Fe_3O_4 treated cells maintained >90% viability at the concentration that inhibited bacterial growth (Fig. 8a). Furthermore, Fe_3O_4 nanoparticle alone treated cells demonstrated >90% viability even in the highest treatment concentration tested (0.008%), whilst commercial CHX diacetate treated cells were not viable. This demonstrates that Fe_3O_4 nanoparticles were not cytotoxic to the fibroblastic cells (Fig. 8a). Magnetic targeted superparamagnetic iron oxide nanoparticles have been shown to be active against *Staphylococcus epidermidis* biofilms and may be an effective alternative to antibiotics for antibiotic-resistant strains [3]. They also appear more effective in penetrating and inhibiting biofilms compared with traditional antibiotics [9]. The antibacterial mechanisms associated with metal nanoparticles include their electrostatic attraction to the negatively charged bacterial cell membrane, their high surface area to volume particle ratio [31]

and production of a reactive oxygen species, ensuring intimate membrane contact and leading to functional disorder of the bacterial cells [3]. The dynamic series of interfacial interactions between nanoparticles and biological structures are however very complex [32].

The crystallization of the CHX compound onto the Fe_3O_4 nanoparticles in the present study is advantageous as it presents an opportunity for a dual and tailored antibacterial effect. Enhanced antibacterial activity might also be obtained through the release of Fe_3O_4 nanoparticles through the dissolution of CHX from the sphere structure. Such a possibility would be valuable in treating antibiotic resistant bacterial biofilms but remains to be demonstrated.

Functionalization of the CHX spheres using the Fe_3O_4 nanoparticles appeared to dramatically decrease the mean (SD) CHX particle diameter from 17.15 (1.99) µm for the particles with no functionalization (Figs. 2a, 2e) to 10.39 (2.61) µm for the CHX/Fe_3O_4 spheres (Figs. 2b, 2f). However, the spherical morphology and structure appeared unchanged (Figs. 2c-f). These metal ions may also act as sites for CHX crystallization, where the co-precipitation system encourages surface crystallization. Previous work indicated that functionalizing the CHX spheres with gold nanorods resulted in correlation between the number of nanoparticles added and the mean CHX particle diameter and number (r^2=0.98) [24]. It is hypothesized that this might be possible with a number of metal ions including Fe_3O_4. The present work was directed towards the magnetic properties associated with ferrimagnetic domains in the Fe_3O_4 structure (tetrahedral and octahedral sub-lattices) [29], enabling a magnetic responsive drug release behavior. The Fe_3O_4 nanoparticles identified in this study are known to interact with each other and problems have been posed with functionalizing these particles for different applications [33]. Domains of the excess Fe_3O_4 nanoparticles were identified trapped within the CHX crystal structure (Figs. 2d, 2f, 3), which enhanced the magnetic effect and allowed the CHX/Fe_3O_4 particle movement.

The spherical CHX particles produced by co-precipitation of $CaCl_2$ and chlorhexidine diacetate had a very high drug content (> 90 wt.%). After TGA analysis (Fig. 4) the remaining weight of the spherical CHX particles was 8.5 wt.%, which was ascribed to the presence of $CaCl_2$ and chlorhexidine diacetate/degradation products [23]. When the CHX particles were functionalized with Fe_3O_4 nanoparticles, the remaining weight increased to 33 wt.% (Fig. 4), which was due to the non-decomposing metal nanoparticles at high temperature. Therefore 24.5 wt.% of Fe_3O_4 nanoparticles were calculated to have been incorporated into the CHX particles and this proportionally reduced CHX content may be the reason for the reduced cytotoxicity observed against fibroblastic cells in comparison with CHX at the same concentration (Fig. 8).

Magnetic nanoparticles are largely incorporated within carriers together with drugs resulting in a low drug loading rate [34]. The current strategy overcomes this problem as it was possible to grow the CHX drug (67 wt.%) directly onto the surface of metal nanoparticles and trap them within its structure (Figs. 2d, 2f). There are many studies using magnetic nanoparticles for targeted delivery, but this is the first study to integrate magnetic nanoparticles directly into drug crystals. This method promotes intimate contact between the metal nanoparticles and CHX crystals that can improve both plasmonic [24] and magnetic sensitivity, broadening the range of drug delivery methods. This also allows the potential of varying the Fe_3O_4 nanoparticle content to tailor these properties and to control the size, number and CHX/ Fe_3O_4 sphere ratio via particle crystallisation.

Functionalization of the CHX spheres allowed the particles to be moved in the viscous HEMA-UDMA resin in response to application of an external magnetic force (Figs. 5b, 5c). The resin sample without magnetic exposure presented a homogeneous distribution of CHX/Fe_3O_4 spheres across the SEM cross sectional samples (Figs. 5a, 6a), which were evenly distributed by the resin mechanical mixing prior to curing. There was also no statistical difference ($p>0.05$)

between the number of spheres present in SEM frames 1-3 indicating this to a depth of 141 microns. Following magnetic exposure (5 and 10 mins) there was a significant increase ($p<0.01$) in the number of CHX/ Fe_3O_4 spheres to a depth of 94 microns from the surface (Fig 5b, 5c, 6b, 6c) nearest to the magnet. This represented 43.7%- 57.3% of the CHX/ Fe_3O_4 spheres in the samples (Figs. 6 b, 6c). At a depth >94 microns (Frames 3, Figs. 5b, 5c) from the surface nearest the magnet the CHX/ Fe_3O_4 sphere number was reduced and not significantly different to the CHX/ Fe_3O_4 sphere distribution (frame 3, group 1) with no magnetic exposure (Table 1, $P>0.05$). Clearly with magnetic exposure there was bulk movement of the CHX/ Fe_3O_4 spheres towards the magnet. The strength of the magnetic field was a key factor, and the magnetic field currently used was 400 mT at the magnet surface. Magnetic field strength has been shown to drop rapidly as a function of distance from the surface for Fe_3O_4 nanoparticles incorporated in microcapsules (1.3 um diameter) and dispersed in cell suspensions [35]. The current work necessitated the movement of the larger mean (SD) 10.39 (2.61) µm diameter CHX/ Fe_3O_4 spheres through a viscous HEMA-UDMA resin and with a Mylar film (1 mm depth) used in the disc fabrication process, further reducing the magnetic fields influence. This would explain the residual CHX/ Fe_3O_4 spheres remaining in the SEM frames furthest away from the magnet (Figs 6 b, 6c). Further work is required on the type of magnet/magnetic field strength and duration on the movement of the drug particles to optimise this process. More efficient synthesis of cubic nanoparticles could also affect their magnetic sensitivity [36], allowing a stronger magnetic field to be used to reduce the exposure time. Guardia et al [37] suggested that cube-shaped (polydispersity <20%) Fe_3O_4 nanoparticles (19 nm) were in the transition between superparamagnetic and ferromagnetic particles, which yields high magneto-thermal properties. The magnetic attraction of CHX/ Fe_3O_4 spheres and their directed movement through a dental polymer or gel is extremely desirable, as it allows the drug to be moved to the infection site to potentially kill the bacteria more efficiently. Antibacterial agents of this kind

navigated by an external magnetic field resulted in an 8-fold higher antibacterial effectiveness in comparison to using antibiotics [3]. The current CHX/ Fe_3O_4 spheres might therefore be effective in sites in the oral cavity inaccessible to current antimicrobial agents, such as deep periodontal pockets or sites susceptible to secondary caries.

The release kinetics of CHX/ Fe_3O_4 spheres from the HEMA-UDMA resin demonstrated a twostage process. Utilising a magnetic field (5 and 10 mins) to draw the CHX/ Fe_3O_4 spheres to the surface appeared to have the effect of inducing a more rapid drug release in the initial stages (until 200 h) from 2.9% (no magnetic field) to 4.0% (5 min) or 4.5% (10 min) (Fig. 7). Near surface drug entrapment and rapid leaching in water explains this burst effect [38, 39]. Inhibition of the polymerisation process by the increased CHX content in the near specimen surface (94 μm) and the presence of residual monomers /unreacted hydrophilic components encouraging water sorption of the polymer [40, 41]. After a 650 h sustained CHX release the overall drug content was also increased from 4.4% to 7.4% (10 min magnetic exposure). Most of the CHX incorporated in the Group 1 resin discs remained in the resin due to the homogeneous distribution of CHX/ Fe_3O_4 spheres throughout the sample interior (Group 1, Fig 5a), which limited the volume fraction of CHX/ Fe_3O_4 spheres available for rapid dissolution and diffusion mechanisms near the surface [41]. Synthesis of spherical CHX particles (without functionalization) by co-precipitation of $CaCl_2$ and chlorhexidine diacetate indicated that the particles were stable, less soluble and with lower CHX release rates than the chlorhexidine diacetate counterpart when dispersed in resin [23]. This can be attributed to Cl^- ions in their structure [42] and has been linked to the CHX release kinetics [22]. Following application of a magnetic field for 5-10 mins the CHX/ Fe_3O_4 spheres (43.7%- 57.3%) were drawn to a depth of 94 microns from the surface of the polymer (Fig 5b, 5c, 6b, 6c). The diffusion of CHX is determined by the water droplets formed around the drug particles, which

form pathways or channels linked to the surface [43]. It is therefore not surprising that the resin discs with more CHX/ Fe_3O_4 spheres distributed near the surface had higher release rates. Mechanisms for CHX/ Fe_3O_4 sphere dissolution appeared to be via the central part of the particle which was more prevalent for spheres nearer the resin surface than the interior. This dissolution behavior was thought to be associated with the penetration and intimate contact between the resin and the interior CHX/ Fe_3O_4 sphere structure [23]. The magnetic CHX/ Fe_3O_4 spheres embedded in resin could therefore also be further triggered with an alternating magnetic field to induce a responsive release [33, 44, 45], which will be explored in future work.

The functionalized CHX spheres (CHX/ Fe_3O_4) have a number of potential applications and this is the first study to demonstrate novel magnetic functionalized CHX particles, where their distribution in a resin can be manipulated with an external magnetic field to alter the CHX release kinetics. These particles could be incorporated into dental filling materials and used to restore exposed implant surfaces or dispersed into maxillo-facial/ denture lining materials, allowing magnetically directed and drug responsive properties. These magnetic CHX/ Fe_3O_4 spheres dispersed in gels and varnishes etc. are particularly attractive for the treatment of persistent periodontal or biomaterial-implant-associated infections.

Acknowledgements

The authors thank Mr. Russell Bailey of Nanovision (QMUL) for help with SEM. Dong Luo thanks for the financial support from the China Scholarship Council during his PhD study. The authors would like to thank Adam Daykin and Queen Mary Innovation for providing funding via the Life Sciences Initiative Proof of Concept Fund.

References

[1] Xiong MH, Bao Y, Yang XZ, Zhu YH, Wang J. Delivery of antibiotics with polymeric particles. Adv Drug Deliver Rev 2014;78:63-76.

[2] Xie S, Tao Y, Pan Y, Qu W, Cheng G, Huang L, et al. Biodegradable nanoparticles for intracellular delivery of antimicrobial agents. J Control Release 2014;187C:101-17.

[3] Subbiahdoss G, Sharifi S, Grijpma DW, Laurent S, van der Mei HC, Mahmoudi M, et al. Magnetic targeting of surface-modified superparamagnetic iron oxide nanoparticles yields antibacterial efficacy against biofilms of gentamicin-resistant staphylococci. Acta Biomater 2012;8:2047-55.

[4] Koldsland OC, Scheie AA, Aass AM. Prevalence of peri-implantitis related to severity of the disease with different degrees of bone loss. J Periodontol 2010;81:231-8.

[5] Valderrama P, Thomas G. Detoxification of implant surfaces affected by peri-implant disease: an overview of surgical methods. Int J Dent 2013;2012:1-9.

[6] Charalampakis G, Rabe P, Leonhardt A, Dahlén G. A follow-up study of peri-implantitis cases after treatment. J Clin Periodontol 2011; 38: 864-871.

[7] Brunthaler A, Konig F, Lucas T, Sperr W, Schedle A. Longevity of direct resin composite restorations in posterior teeth. Clin Oral Invest 2003;7:63-70.

[8] Wang Z, Shen Y, Haapasalo M. Dental materials with antibiofilm properties. Dent Mater 2014;30:e1-16.

[9] Taylor EN, Kummer KM, Durmus NG, Leuba K, Tarquinio KM, Webster TJ. Superparamagnetic iron oxide nanoparticles (SPION) for the treatment of antibiotic-resistant biofilms. Small 2012;8:3016-27.

[10] Lu ZH, Prouty MD, Guo ZH, Golub VO, Kumar CSSR, Lvov YM. Magnetic switch of permeability for polyelectrolyte microcapsules embedded with Co@Au nanoparticles. Langmuir 2005;21:2042-50.

[11] Patra S, Roy E, Karfa P, Kumar S, Madhuri R, Sharma PK. Dual-responsive polymer coated superparamagnetic nanoparticle for targeted drug delivery and hyperthermia treatment. ACS Appl Mater Inter 2015;7:9235-46.

[12] Yu J, Ju Y, Zhao L, Chu X, Yang W, Tian Y, et al. Multistimuli-regulated photochemothermal cancer therapy remotely controlled via Fe5C2 Nanoparticles. ACS Nano 2016;10:159-69.

[13] Pavlov AM, Gabriel SA, Sukhorukov GB, Gould DJ. Improved and targeted delivery of bioactive molecules to cells with magnetic layer-by-layer assembled microcapsules. Nanoscale 2015;7:9686-93.

[14] Hao R, Xing R, Xu Z, Hou Y, Gao S, Sun S. Synthesis, functionalization, and biomedical applications of multifunctional magnetic nanoparticles. Adv Mater 2010;22:2729-42.

[15] Perez RA, Patelab KD, Kim HW. Novel magnetic nanocomposite injectables: calcium phosphate cements impregnated with ultrafine magnetic nanoparticles for bone regeneration. RSC Adv 2015;5:13411-19.

[16] Yun HM, Ahn SJ, Park KR, Kim MJ, Kim JJ, Jin GZ, et al. Magnetic nanocomposite scaffolds combined with static magnetic field in the stimulation of osteoblastic differentiation and bone formation. Biomaterials 2016;85:88-98.

[17] Yun HM, Kang SK, Singh RK, Lee JH, Lee HH, Park KR, et al. Magnetic nanofiber scaffold-induced stimulation of odontogenesis and pro-angiogenesis of human dental pulp cells through Wnt/MAPK/NF-kappaB pathways. Dent Mater 2016;32:1301-11.

[18] Dabbagh A, Abu Kasim NH, Bakri MM, Wakily H, Ramasindarum C, Abdullah BJJ. Polyethylene-glycol coated maghemite nanoparticles for treatment of dental hypersensitivity. Mater Lett 2014;121:89-92.

[19] Mahmoudi M, Serpooshan V. Silver-coated engineered magnetic nanoparticles are promising for the success in the fight against antibacterial resistance threat. ACS Nano 2012;6:2656-64.

[20] Wu J, Weir MD, Melo MA, Xu HH. Development of novel self-healing and antibacterial dental composite containing calcium phosphate nanoparticles. J Dent 2015;43:317-26.

[21] Tabary N, Chai F, Blanchemain N, Neut C, Pauchet L, Bertini S, et al. A chlorhexidine-loaded biodegradable cellulosic device for periodontal pockets treatment. Acta Biomater 2014;10:318-29.

[22] Luo D, Shahid S, Wilson RM, Cattell MJ, Sukhorukov GB. Novel formulation of chlorhexidine spheres and sustained release with multilayered encapsulation. ACS Appl Mater Inter 2016;8:12652-60.

[23] Luo D, Shahid S, Sukhorukov GB, Cattell MJ. Synthesis of novel chlorhexidine spheres with controlled release from a UDMA-HEMA resin using ultrasound. Dent Mater 2017;33:713-22.

[24] Luo D, Hasan MS, Shahid S, Khlebtsov B, Cattell MJ, Sukhorukov GB. Gold nanorod mediated chlorhexidine microparticle formation and near-infrared light induced release. Langmuir 2017;33:7982-93.

[25] Sheparovych R, Sahoo Y, Motornov M, Wang S, Luo H, Prasad PN, et al. Polyelectrolyte stabilized nanowires from Fe_3O_4 nanoparticles via magnetic field induced self-assembly. Chem Mater 2006;18:591-3.

[26] Luo D, Zhang X, Shahid S, Cattell MJ, Gould DJ, Sukhorukov GB. Electrospun poly(lactic acid) fibers containing novel chlorhexidine particles with sustained antibacterial activity. Biomater Sci 2016;5:111-19.

[27] Hajipour MJ, Fromm KM, Ashkarran AA, Jimenez de Aberasturi D, de Larramendi IR, Rojo T, et al. Antibacterial properties of nanoparticles. Trends Biotechnol 2012;30:499-511.

[28] Neel L. Proprietes magnetiques des ferrites-ferrimagnetisme et antiferromagnetisme. Ann Phys 1948;3:137-98.

[29] Parkinson GS. Iron oxide surfaces. Surf Sci Rep 2016;71:272-365.

[30] Nie S, Starodub E, Monti M, Siegel DA, Vergara L, Gabaly FE, et al. Insight into magnetite's redox catalysis from observing surface morphology during oxidation. J Am Chem Soc 2013;135:10091-8.

[31] Allaker RP. The use of nanoparticles to control oral biofilm formation. J Dent Res 2010;89:1175-86.

[32] Nel AE, Madler L, Velegol D, Xia T, Hoek EMV, Somasundaran P, et al. Understanding biophysicochemical interactions at the nano-bio interface. Nat Mater 2009;8:543-57.

[33] Kakwere H, Leal MP, Materia ME, Curcio A, Guardia P, Niculaes D, et al. Functionalization of strongly interacting magnetic nanocubes with (thermo) responsive coating and their application in hyperthermia and heat-triggered drug delivery. ACS Appl Mater Inter 2015;7:10132-45.

[34] Peça IN, Bicho A, Gardner R, Cardoso MM. Control of doxorubicin release from magnetic Poly(dl-lactide-co-glycolide) nanoparticles by application of a non-permanent magnetic field. J Nanopart Res 2015;17:427.

[35] Pavlov AM, De Geest BG, Louage B, Lybaert L, De Koker S, Koudelka Z, et al. Magnetically engineered microcapsules as intracellular anchors for remote control over cellular mobility. Adv Mater 2013;25:6945-50.

[36] Kim D, Lee N, Park M, Kim BH, An K, Hyeon T. Synthesis of uniform ferrimagnetic magnetite nanocubes. J Am Chem Soc 2009;131:454-5.

[37] Guardia P, Corato RD, Lartigue L, Wilhelm C, Espinosa A, Garcia-Hernandez M, et al. Water-soluble iron oxide nanocubes with high values of specific absorption rate for cancer cell hyperthermia treatment. ACS Nano 2012;6:3080-91.

[38], Riggs PD, Braden M, Patel, M. Chlorhexidine release from room temperature polymerising methacrylate systems. Biomaterials 2000;21:345-51.

[39] Huang X, Brazel CS. On the importance and mechanisms of burst release in matrix-controlled drug delivery systems. J Control Release 2001;73:121-36.

[40] Wilson SJ, Wilson HJ. The release of chlorhexidine from modified dental acrylic resin. J Oral Rehabil 1993;20:311-9.

[41] Hiraishi N, Yiu CK, King NM, Tay FR. Chlorhexidine release and antibacterial properties of chlorhexidine-incorporated polymethyl methacrylate-based resin cement. J Biomed Mater Res B 2010;94:134-40.

[42] Zeng P, Rao A, Wiedmann TS, Bowles W. Solubility properties of chlorhexidine salts. Drug Dev Ind Pharm 2009;35:172-76.

[43] Leung D, Spratt DA, Pratten J, Gulabivala K, Mordan NJ, Young AM. Chlorhexidine-releasing methacrylate dental composite materials. Biomaterials 2005;26:7145-53.

[44] Guisasola E, Baeza A, Talelli M, Arcos D, Moros M, de la Fuente JM, et al. Magnetic-responsive release controlled by hot spot effect. Langmuir 2015;31:12777-82.

[45] Griffete N, Fresnais J, Espinosa A, Wilhelm C, Bée A, Ménager C. Design of magnetic molecularly imprinted polymer nanoparticles for controlled release of doxorubicin under an alternative magnetic field in athermal conditions. Nanoscale 2015;7:18891-6.

List of Figures

Figure 1

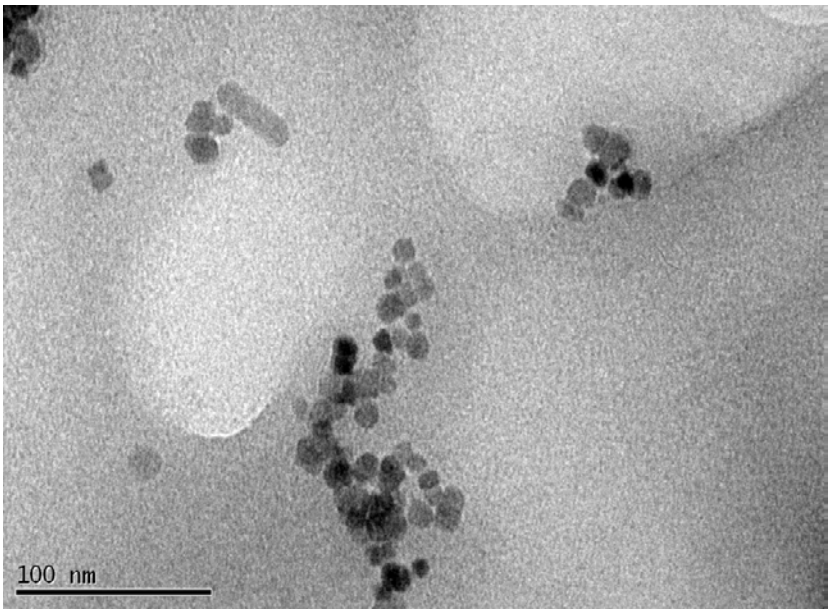

Figure 2

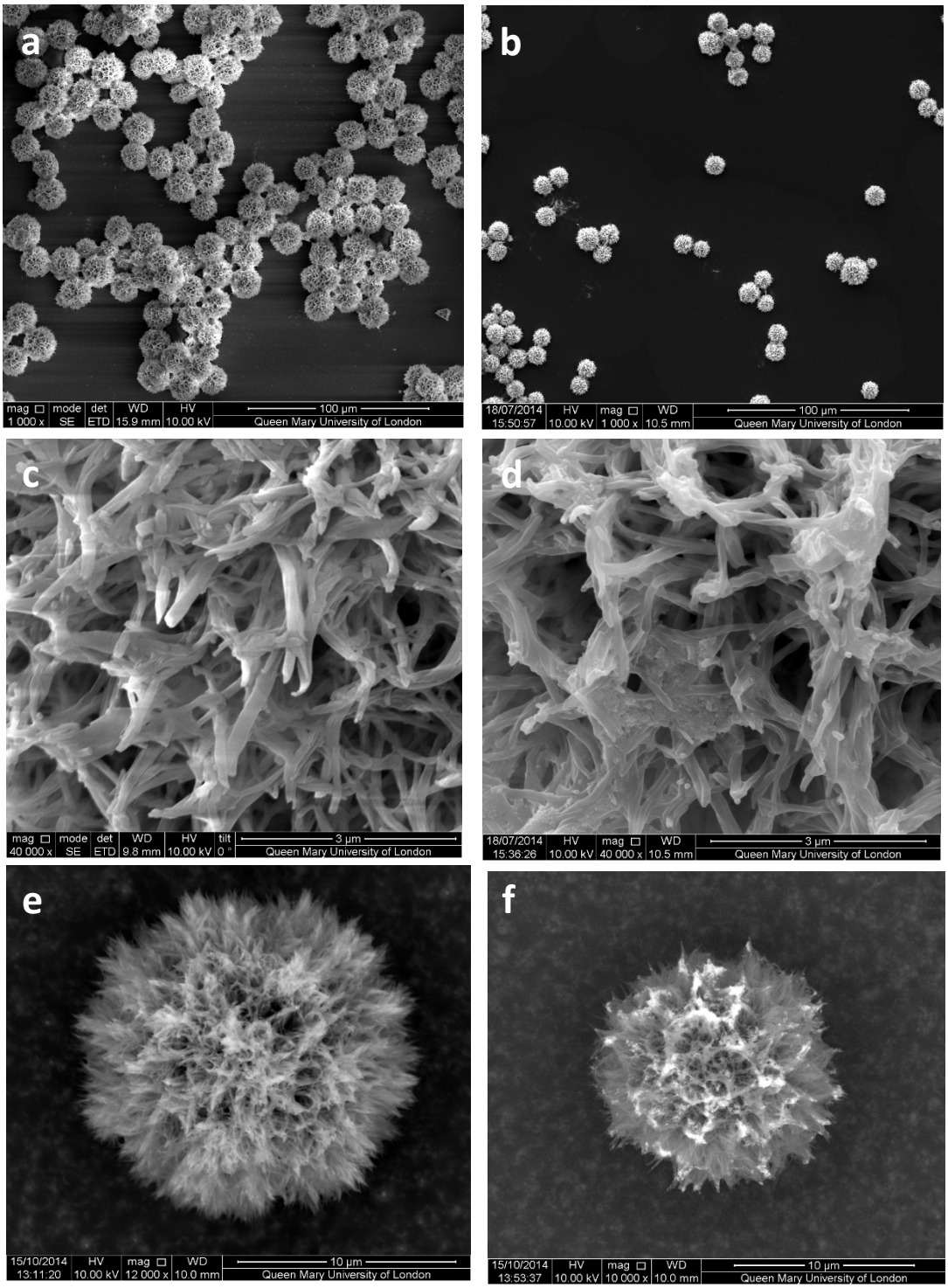
a
mag 1 000 x | mode SE | det ETD | WD 15.9 mm | HV 10.00 kV | 100 µm | Queen Mary University of London
b
18/07/2014 15:50:57 | HV 10.00 kV | mag 1 000 x | WD 10.5 mm | 100 µm | Queen Mary University of London
c
mag 40 000 x | mode SE | det ETD | WD 9.8 mm | HV 10.00 kV | tilt 0 ° | 3 µm | Queen Mary University of London
d
18/07/2014 15:36:26 | HV 10.00 kV | mag 40 000 x | WD 10.5 mm | 3 µm | Queen Mary University of London
e
15/10/2014 13:11:20 | HV 10.00 kV | mag 12 000 x | WD 10.0 mm | 10 µm | Queen Mary University of London
f
15/10/2014 13:53:37 | HV 10.00 kV | mag 10 000 x | WD 10.0 mm | 10 µm | Queen Mary University of London

Figure 3

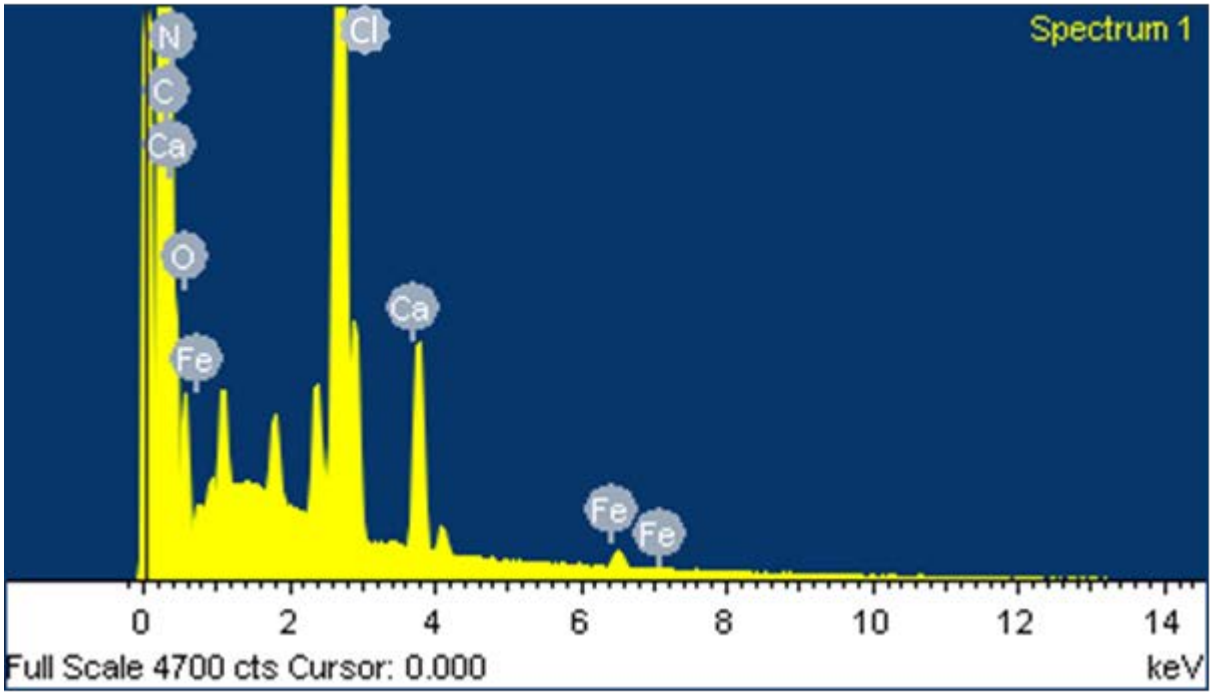
Spectrum 1
N
C
Ca
O
Fe
Cl
Ca
Fe
Fe
0
2
4
6
8
10
12
14
Full Scale 4700 cts Cursor: 0.000
keV

Figure 4

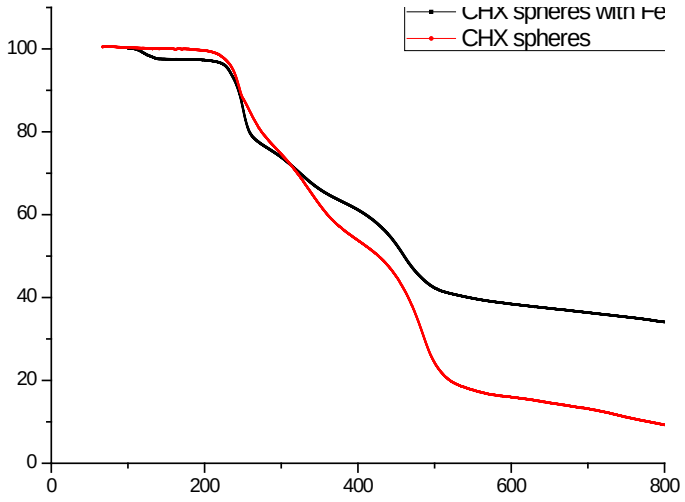
CHX spheres with Fe
CHX spheres
100
80
60
40
20
0
0
200
400
600
800

Figure 5

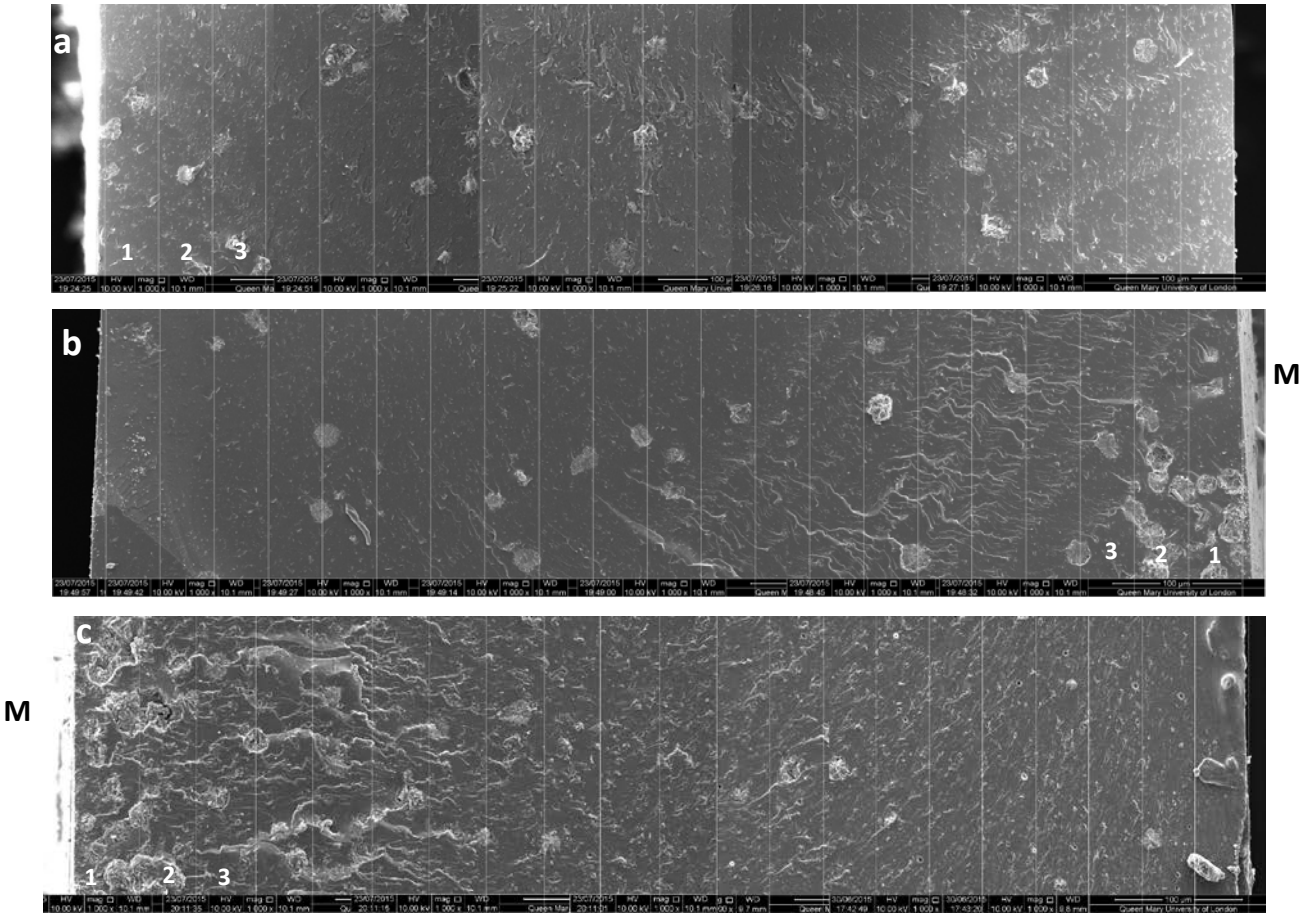

Figure 6a

a

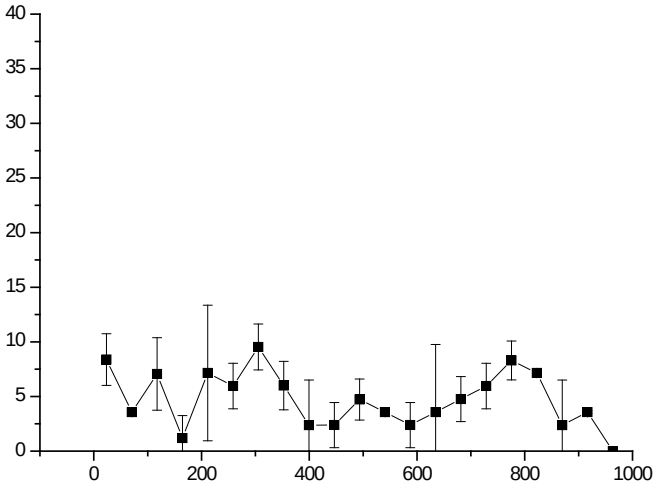

Figure 6b

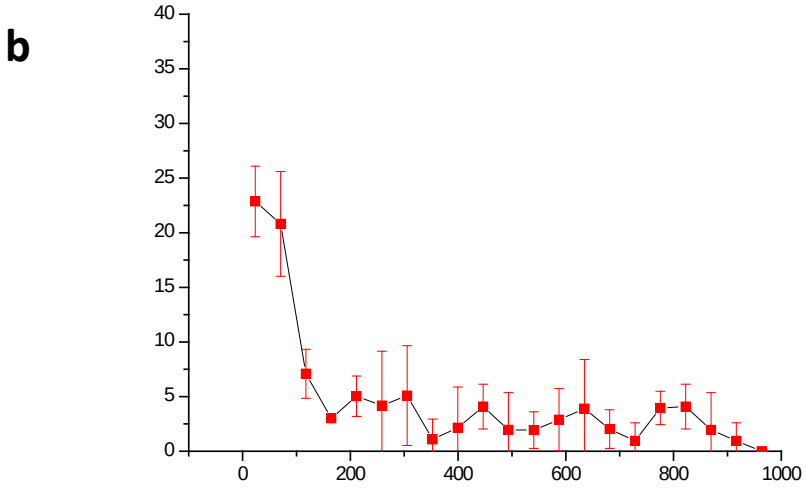

Figure 6c

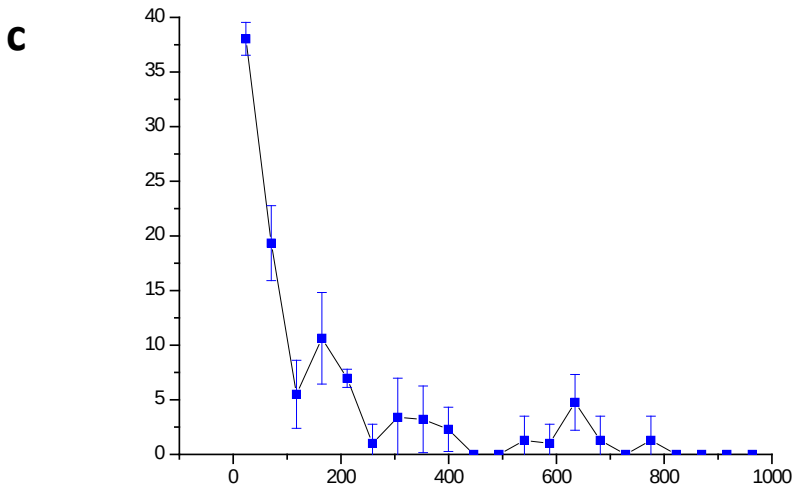

Figure 7

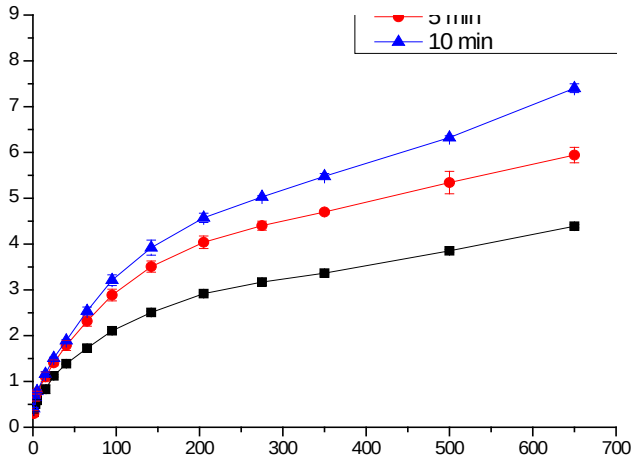

Figure 8

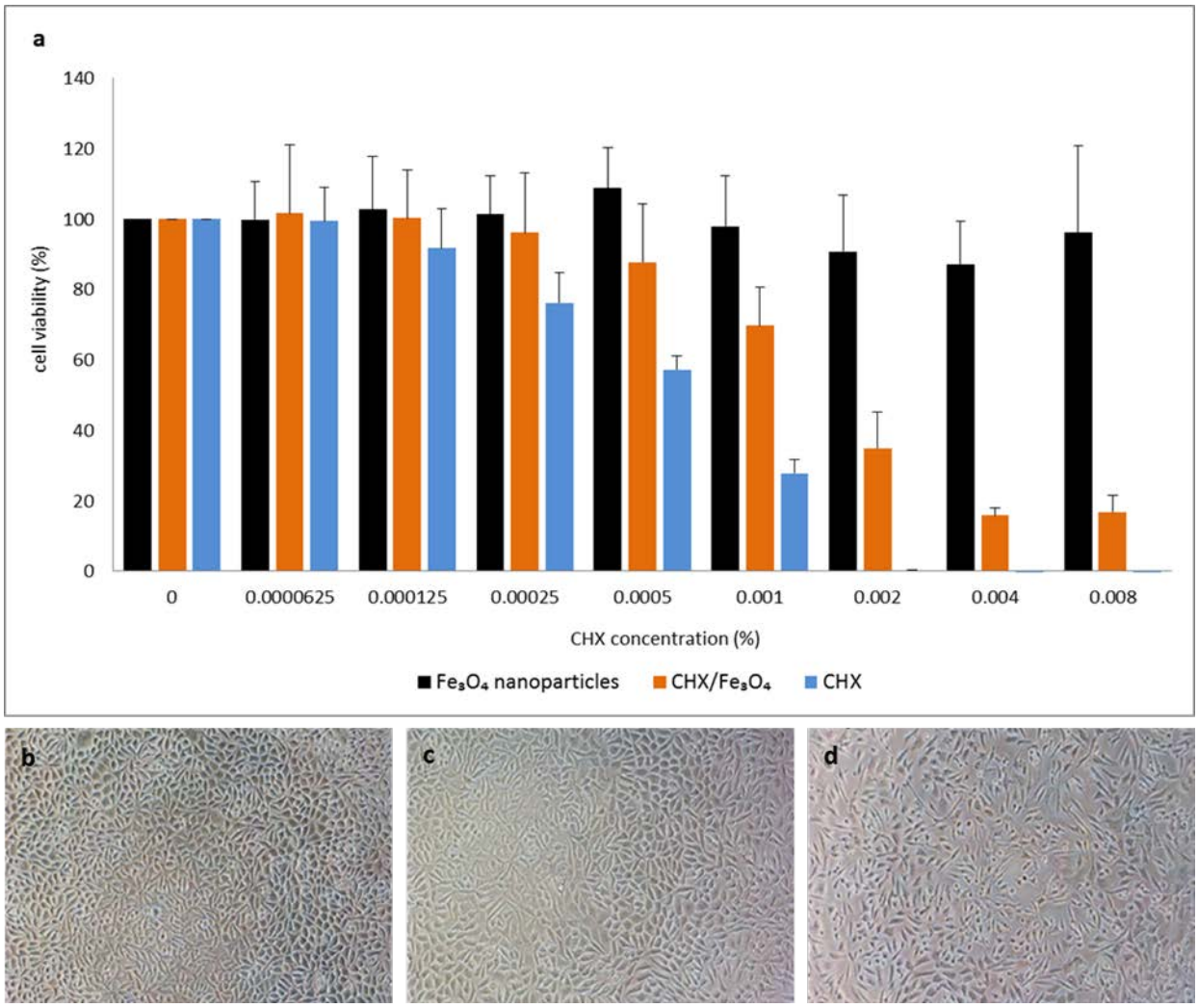
a
140
120
100
80
60
40
20
0
cell viability (%)
0
0.0000625
0.000125
0.00025
0.0005
0.001
0.002
0.004
0.008
CHX concentration (%)
Fe3O4 nanoparticles
CHX/Fe3O4
CHX
b
c
d

Figure 9

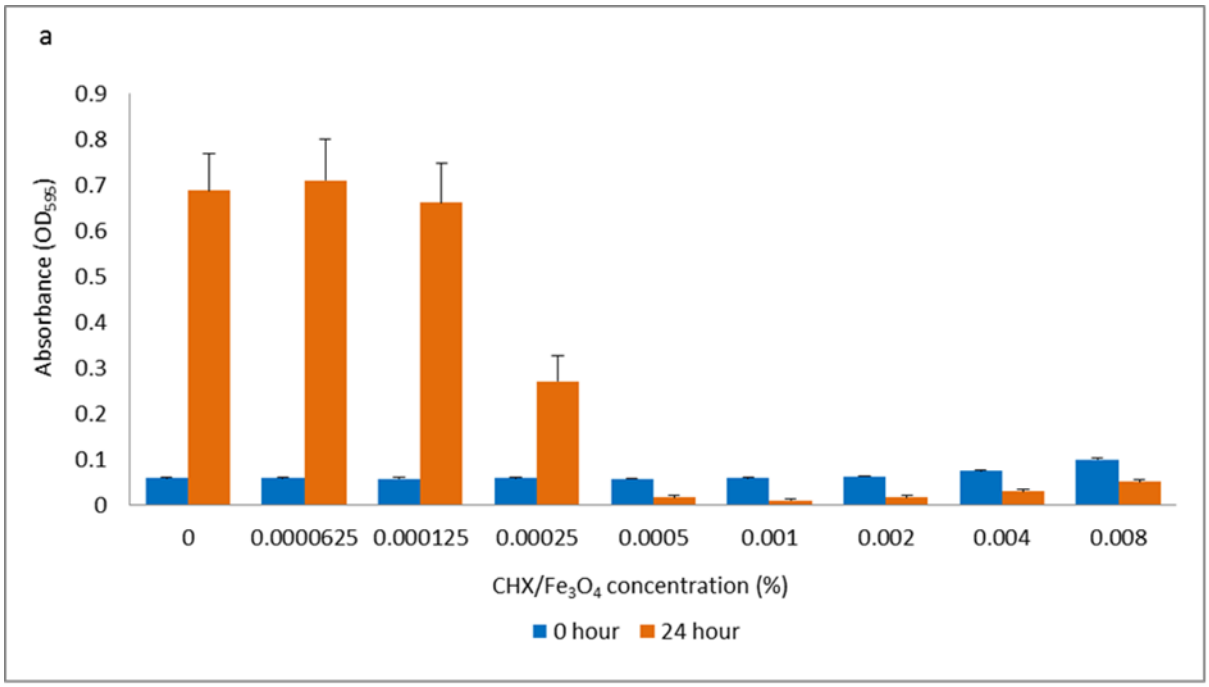
a
Absorbance (OD_{595})
0.9
0.8
0.7
0.6
0.5
0.4
0.3
0.2
0.1
0
0
0.0000625
0.000125
0.00025
0.0005
0.001
0.002
0.004
0.008
CHX/Fe_3O_4 concentration (%)
0 hour
24 hour

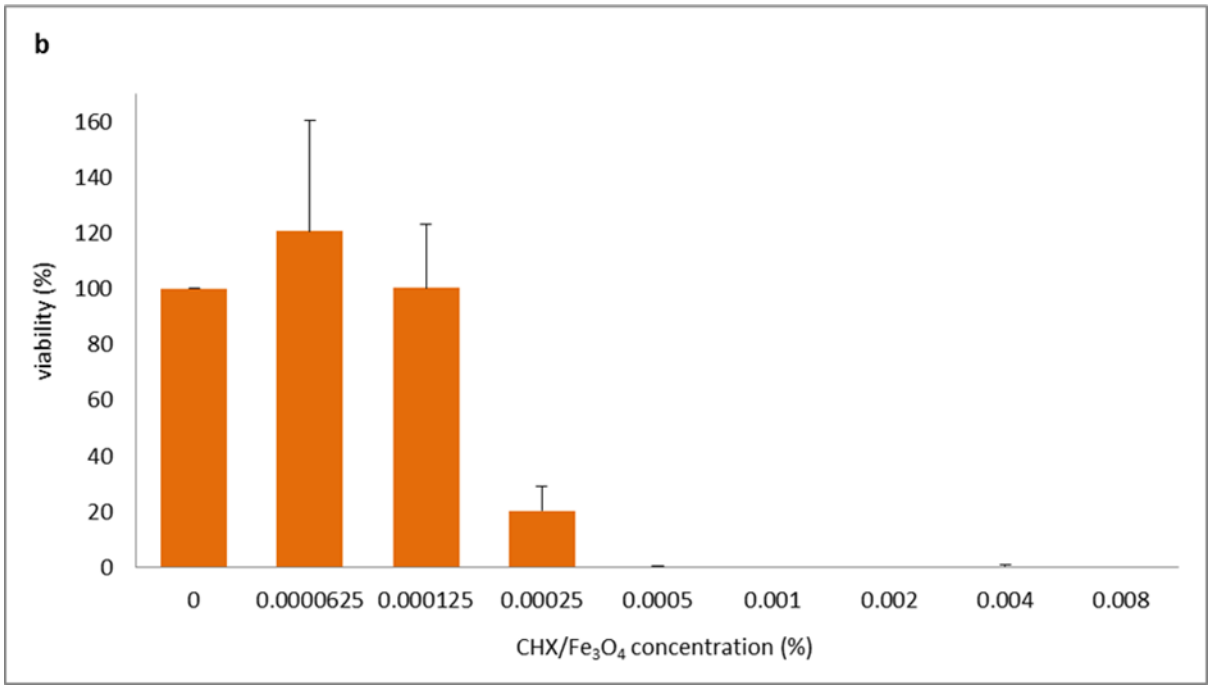
b
viability (%)
160
140
120
100
80
60
40
20
0
0
0.0000625
0.000125
0.00025
0.0005
0.001
0.002
0.004
0.008
CHX/Fe_3O_4 concentration (%)

List of Tables

Table 1

SEM Frame Sections	Mean Particle Number (SD) (Group 1)	Mean Particle Number (SD) (Group 2)	Mean Particle Number (SD) (Group 3)
1	**2.3 (0.6) [a,c,e,f]**	**7.7 (1.5) [b,d]**	**11 (1.0) [d]**
2	**1.0 (0.0) [a,c,f]**	**7.0 (2.0) [b]**	**5.7 (1.5) [b,e]**
3	**2.0 (1.0) [a,c,f]**	**2.3 (0.6) [c,e, f]**	**1.7 (1.2) [f]**

*Significant differences are indicated by different superscript letters between groups ($P<0.05$). (Figures are based on n=3 panoramic images per test group).